

# Hydrodynamics of a Relativistic Fireball: the Complete Evolution

Shiho Kobayashi, Tsvi Piran and Re'em Sari

Racah Institute of Physics, The Hebrew University, Jerusalem, 91904 Israel

Received \_\_\_\_\_; accepted \_\_\_\_\_

arXiv:astro-ph/9803217v1 18 Mar 1998

## ABSTRACT

We study numerically the evolution of an adiabatic relativistic fireball expanding into a cold uniform medium. We follow the stages of initial free expansion and acceleration, coasting and then deceleration and slowing down to a non-relativistic velocity. We compare the numerical results with simplified analytical estimates. We show that the relativistic self similar Blandford-McKee solution describes well the relativistic deceleration epoch. It is an excellent approximation throughout the relativistic deceleration stage, down to  $\gamma \sim 5$ , and a reasonable approximation even down to  $\gamma \sim 2$  though the solution is rigorous only for  $\gamma \gg 1$ . We examine the transition into the Blandford-McKee solution, and the transition from the solution to the non-relativistic self similar Sedov-Taylor solution. These simulations demonstrate the attractive nature of the Blandford-McKee solution and its stability to radial perturbations.

*Subject headings:* hydrodynamics — relativity — shock waves — gamma-ray bursts

## 1. Introduction

Sedov (1946), Taylor (1950) and Von Neumann (1947) discovered, in the forties, a self similar solution of the strong explosion problem, in which a large amount of energy is released on a short time scale in a small volume. This solution is known today as the “Sedov-Taylor” self similar solution. It describes a shock wave propagating into a uniform density surrounding. The shock wave and the matter behind it decelerate as more and more mass is collected. This solution describes well the adiabatic stage of a supernova remnant evolution.

Blandford and McKee (1977) have later established a self similar solution describing the extreme relativistic version of the strong explosion problem. In this solution the Lorentz factor of the shock and the fluid behind it is much larger than unity. Such high Lorentz factors arise if the rest mass contained within the region where the energy  $E$  was released is much smaller than  $E$ . In other words when the region containing the energy is “radiation dominated” rather than matter dominated. Such a region was later termed a “fireball”.

Cavallo and Rees (1978) have considered the physical processes relevant in a radiation dominated fireball as a model for gamma-ray bursts (GRBs). Goodman (1986) and Paczyński (1986) have then considered the evolution of such a fireball. They have shown that initially the radiation-pair plasma in a purely radiative fireball behaves like a fluid and it expands and accelerates under its own pressure until the local temperature drops to  $\sim 20\text{keV}$ , when the last pairs annihilate and the fireball becomes optically thin. Later Shemi and Piran (1990) considered matter contaminated fireballs. They have shown that, quite generally, all the initial energy will be transferred to the baryons in such fireballs whose final outcome is a shell of relativistic freely expanding baryons. Piran, Shemi and Narayan (1993) and Mészáros Laguna and Rees (1993) have later carried these calculations in greater details. These works show that an initially homogeneous fireball will first accelerate

while expanding and then coast freely as all its internal energy was transformed to kinetic energy.

The surrounding matter will eventually influence the fireball after enough external matter has been collected and most of the energy has been transferred from the shell to the ISM. If the surrounding matter is diluted enough, then this will take place only after the initial free acceleration phase. This influence was considered by Mészáros and Rees (1992), and Katz (1993), who suggested that the GRB is produced during this stage. The detailed shock evolution was later studied by Sari and Piran (1995). It is only after these stages, that the fireball has given the ISM most of its energy and then the self-similar deceleration solution of Blandford-McKee applies. When the shock decelerates enough so that it is no longer relativistic, it is described by the Sedov-Taylor solution.

Today it is widely accepted that GRBs involve relativistic expanding matter of this kind. While the GRB itself is produced, most likely, via internal shocks (Narayan, Paczyński & Piran, 1992; Rees & Mészáros, 1994; Sari & Piran, 1997). The observed GRB afterglow corresponds, on the other hand, to the slowing down of this relativistic flow. This has led to an increasing interest in the fireball solution and in its various regimes. In this paper we study the evolution of a homogeneous fireball focusing on its interaction with the surrounding matter. We do not consider here internal shocks, which arise due to interaction within the relativistic flow and require nonuniform velocity.

We have developed a spherically symmetric relativistic Lagrangian code based on a second-order Godunov method with an exact Riemann solver to solve the ultra-relativistic hydrodynamics problem. With this code, it is possible to track the full hydrodynamical evolution of the fireball within a single computation, from its initial “radiation dominated” stage at rest through its acceleration, coasting, and shock formation, up to the relativistic deceleration and finally to the Newtonian deceleration. With typical parameters this

computation spans more than eight orders of magnitudes in the size of the fireball and more than twenty orders of magnitudes in its density. We describe these computations here. We show that, quite generically, the solution converges during the relativistic deceleration phase to the Blandford-McKee solution and then it transforms to the Sedov-Taylor solution. Even though the attractive nature of the Blandford-McKee solution suggests that it is stable we explore explicitly the stability of this solution and we show that it is stable to radial perturbations.

We review, first, in section 2 the current analytic understanding of the fireball evolution thorough the following stages: (i) free acceleration and coasting, (ii) energy transfer (iii) relativistic self similar solution and (iv) Newtonian Sedov-Taylor solution. We discuss the numerical results in section 3. In section 4 we examine the evolution of perturbations to the Blandford-McKee solution. We discuss the implications of these results in section 5.

## 2. Analytic Estimates

The evolution of a fireball is characterized by several phases. The transitions between these phases are determined by several critical radii that are summarized in table 1.

Table 1: *Critical Radii*

$R_0$	Initial Fireball Size	
$R_L$	Coasting	$R_0\eta$
$R_s$	Spreading (and Internal Shocks)	$R_0\eta^2$
$R_\Delta$	External Shocks (the NRS Case)	$l^{3/4}\Delta^{1/4}$
$R_\gamma$	External Shocks (the RRS Case)	$l/\eta^{2/3}$
$R_N$	Relativistic Reverse Shock	$l^{3/2}/\Delta^{1/2}\eta^2$
$l$	Sedov Length	$(E/\rho_1)^{1/3}$

## 2.1. Free Acceleration and Coasting

We consider a homogeneous fireball of energy  $E$  and a baryonic load of total mass  $M_0$  confined initially in a sphere of radius  $R_0$ . We define the dimensionless entropy (or the initial random Lorentz factor)  $\eta \equiv E/M_0$ . This fireball expands into a surrounding low density medium (with a density  $\rho_1$ ) which we will refer to as the ISM. This can be considered to be a free expansion in its initial stage. After a short acceleration phase, the motion becomes highly relativistic. Conservations of baryon number, energy and momentum yield the following conservation laws along a null flow line of each fluid element in the shell (Piran, Shemi & Narayan, 1993):

$$r^2 \rho \gamma, \quad r^2 p^{3/4} \gamma \quad \text{and} \quad r^2 (4p + \rho) \gamma^2 = \text{constant}, \quad (1)$$

where  $r(t)$ ,  $\gamma(t)$ ,  $p(t)$  and  $\rho(t)$  are the radius, Lorentz factor, pressure and rest mass density of the fluid element, respectively. In this paper, distance, time, velocity and the corresponding Lorentz factors are measured in the observer frame. Thermodynamic quantities ( $p$  and  $\rho$ ) are measured in the local fluid frame. We use units in which the speed of light  $c = 1$ . The above equations assume an adiabatic gas index of  $4/3$ .

Initially the fireball is extremely hot ( $p \gg \rho$ ), so that equation (1) yields

$$\gamma \propto r, \quad \rho \propto r^{-3} \quad \text{and} \quad p \propto r^{-4}, \quad (2)$$

(Goodman, 1986; Paczyński, 1986; Shemi & Piran, 1990). The fireball is approximately homogeneous in the local frame, but due to relativistic effects it appears to an observer at rest as a narrow shell with a radial width  $\Delta \sim r/\gamma \sim R_0$  (Shemi & Piran, 1990; Piran, Shemi & Narayan, 1993). As the fireball expands, the internal energy is converted into kinetic energy of the baryons. At the radius  $R_L \equiv \eta R_0$ , the fireball uses up all the internal energy and the approximation  $p \gg \rho$  breaks down. This is the end of the acceleration phase.

Now, the internal energy of the fireball becomes negligible compared to the rest mass energy ( $p \ll \rho$ ), and equation (1) yields

$$\gamma = \text{constant}, \quad \rho \propto r^{-2} \quad \text{and} \quad p \propto r^{-8/3}, \quad (3)$$

(Piran Shemi & Narayan, 1993). The fireball behaves like a pulse of energy with a frozen radial profile propagating at almost the speed of light.

## 2.2. Spreading, The Reverse Shock and Energy Transfer

This frozen pulse approximation on which equation (1) is based breaks down ultimately at the radius  $R_s \equiv R_0 \eta^2$ . Each fluid shell moves with a slightly different velocity and the fireball begins to spread at  $R_s$ . Internal shocks will take place around  $R_s$  if the fireball is inhomogeneous and the velocity is not a monotonic function of the radius. As mentioned earlier, these shocks produce, most likely, the observed GRB. However, even under optimal condition they cannot convert more than about a quarter of the kinetic energy to radiation. Hence even an inhomogeneous shell will continue carrying ample kinetic energy beyond this stage. We consider here only homogeneous fireball. The possible effect of internal shocks on the fireball evolution has been discussed extensively in another papers (Kobayashi, Piran & Sari, 1997; Daigne & Mochkovitch, 1997)

The coasting can also end if the surrounding matter begins to influence the shell. The interaction between the shell and the ISM can be described by two shocks: a forward shock propagating into the ISM and a reverse shock propagating into the shell. Sari and Piran (1995) have defined three critical radii in this respect:  $R_N \equiv l^{3/2} / \Delta^{1/2} \eta^2$  where the energy density produced by the shocks becomes high enough so that the reverse shock is relativistic and begins to reduce the Lorentz factor of the shell considerably;  $R_\Delta \equiv l^{3/4} \Delta^{1/4}$  where the reverse shock crosses the shell; and  $R_\gamma \equiv l / \eta^{2/3}$  where the mass of the shocked ISM is  $M_0 / \eta$ .

Here  $l \equiv (E/\rho_1)^{1/3}$  is the Sedov length. Fortunately, a simple relations between these four radii can be given in terms of the dimensionless variable  $\xi \equiv (l/\Delta)^{1/2}\eta^{-4/3}$ ;

$$\xi^2 R_s = \sqrt{\xi} R_\Delta = R_\gamma = R_N/\xi. \quad (4)$$

If initially  $\xi > 1$  then  $R_s$  is the smallest radius. The shell begins to spread at  $R_s$ . After that the width  $\Delta$  satisfies  $\Delta = r/\gamma^2 \propto r$  and the scaling of the shell parameters becomes

$$\gamma = \text{constant}, \quad \rho \propto r^{-3} \quad \text{and} \quad p \propto r^{-4}. \quad (5)$$

During the spreading phase the value of  $\xi > 1$  decreases. However, as long as  $\xi > 1$  the relation  $R_s < R_\Delta < R_\gamma < R_N$  is valid. When  $\xi \sim 1$  these different radii become comparable: the reverse shock crosses the shell, it becomes mildly relativistic and an ISM mass of  $M_0/\eta$  was collected. Since the reverse shock is just mildly relativistic at this stage, the shell's Lorentz factor have changed only by a factor of order unity. We call this the Newtonian Reverse Shock (NRS) case since the reverse shock is Newtonian relative to the unshocked shell. This is not to be confused with the fact that  $\gamma \gg 1$  in this case and the forward shock is ultra-relativistic.

If initially  $\xi < 1$  then  $R_N$  is the smallest radius. The reverse shock becomes relativistic before it crosses the shell. At  $r > R_N$  the reverse shock begins to reduce considerably the Lorentz factor of the shell's matter that it crosses. The Lorentz factor of the shocked material is

$$\gamma(r) = l^{3/4} \Delta^{-1/4} r^{-1/2} \quad (6)$$

(Sari, 1997). The shell has decelerated significantly by the time that the reverse shock has crossed the shell at  $R_\Delta$ . At this stage, the Lorentz factor was reduced from its initial value of  $\eta$  to  $\eta \xi^{3/4} = (l/\Delta)^{3/8} \ll \eta$ . We call this the Relativistic Reverse Shock (RRS) case as most of the deceleration is done by a strong relativistic reverse shock.

The coasting radius, when the shell begins to coast freely,  $R_L$ , is related to the other radii by a simple relation,  $\eta\xi^2R_L = \xi^2R_s = \sqrt{\xi}R_\Delta = R_\gamma = R_N/\xi$ . In the NRS case  $\xi > 1$  and  $R_L$  is the smallest radius. All the initial thermal energy is converted to kinetic energy before the shell begins to decelerate. In the RRS case ( $\xi < 1$ ) it is possible that the deceleration, due to external matter, begins before all the energy of the fireball was converted to kinetic energy. The conditions  $R_L < R_N$  and  $\xi < 1$  yield  $(l/\Delta)^{3/8} < \eta < \sqrt{l/\Delta}$  (see figure 1):  $\xi$  should be larger than  $(\Delta/l)^{1/6}$  in order that  $R_L < R_N$ . We limit the discussion to this case here,  $R_L < R_N$ , i.e., the fireball transforms all its internal energy to kinetic energy before the ISM begins influence its evolution.

The NRS case is relevant if the initial fireball is small and contains relatively many baryons (equivalently,  $\eta$  is relatively small), while the RRS case is relevant if the fireball is large and it is less polluted by baryon. The shell has given the ISM most of its energy either at  $R_\gamma (= R_N = R_\Delta)$  in the NRS case, or at  $R_\Delta$  in the RRS case,

### 2.3. Relativistic Self Similar Deceleration

For  $r > R_\gamma$  for the NRS case, or  $r > R_\Delta$  for the RRS case, the shocked ISM contains most of the energy  $E$ . From this stage the shell plays a negligible part in the consecutive evolution. The profile of the shocked ISM is determined now just by two parameters,  $E$  and  $\rho_1$ .

When the forward shock reaches a radius  $R$  the fireball has a mass  $4\pi\rho_1R^3/3$ . The energy in the shocked fluid is therefor  $\propto \rho_1R^3\gamma^2$ . Since this equals the total energy of the system  $E$ , we obtain a scaling law,  $\gamma \propto (E/\rho_1)^{1/2}R^{-3/2}$ . The exact proportionality constant depends on the profiles behind the shock. Blandford and McKee (1976) describe an analytic

self similar solution, in which the Lorentz factor, the density and the pressure are given by

$$\gamma(t, r) = \frac{1}{\sqrt{2}}\Gamma\chi^{-1/2}, \quad \rho(t, r) = 2\sqrt{2}\rho_1\Gamma\chi^{-5/4}, \quad p(t, r) = \frac{2}{3}\rho_1\Gamma^2\chi^{-17/12}, \quad (7)$$

where  $\Gamma(t) \equiv \sqrt{17/8\pi}(R/l)^{-3/2}$  is the Lorentz factor of the shock itself, and the similarity variable  $\chi$  is defined by  $\chi(t, r) \equiv 1 + 8\Gamma^2(1 - r/R)$ . The shock radius is given by  $R = R(t) \sim (1 - 1/8\Gamma^2)t$ . In the previous section  $r$  denotes the radius of a fluid element in the shell, but  $r$  and  $t$  are independent coordinates here.

## 2.4. The Sedov-Taylor Solution

The Blandford-McKee self similar solution is derived with the assumption  $\gamma, \Gamma \gg 1$ . This assumption breaks down when the shock sweeps out a volume  $\sim l^3$  of ISM and its motion becomes non-relativistic. At the radius  $l$  the Sedov-Taylor (Sedov, 1946; Von Neumann, 1947; Taylor, 1950) solution becomes a good approximation. A characteristic length scale at a time  $t$ , which we can form from the two parameters  $E$  and  $\rho_1$ , gives the shock radius  $R(t) \equiv \alpha(Et^2/\rho_1)^{1/5}$  within a numerical constant factor  $\alpha$  depending on the adiabatic constant  $\hat{\gamma}$  ( $\alpha = 0.99$  for  $\hat{\gamma} = 4/3$ ). The velocity of the shock is  $u \equiv dR/dt = 2R/5t$ . The velocity  $\beta_2$ , the density  $\rho_2$  and the pressure  $p_2$  just behind the shock can be expressed in terms of  $u$ :  $\beta_2 = 6u/7, \rho_2 = 7\rho_1, p_2 = 6\rho_1u^2/7$  for the adiabatic index  $\hat{\gamma} = 4/3$ . The profile throughout the region behind the shock is given by the velocity  $\beta = 2rV/5t$ , the density  $\rho = \rho_1G$  and the pressure  $p = 3r^2\rho_1GZ/25t^2$  (Landau & Lifshitz, 1987). The dimensionless variables  $V, G, Z$  are functions of the similarity variable  $\zeta \equiv r/R$  only and are given in an implicit analytical form by the following equations:

$$\zeta^5 = \left(\frac{7}{6}V\right)^{-2} \left\{\frac{7}{17}(5 - 3V)\right\}^{-232/99} \left\{\frac{7}{3}(4V - 3)\right\}^{5/11}, \quad (8)$$

$$Z = \frac{2}{3}V^2(1 - V)(4V - 3)^{-1}, \quad (9)$$

$$G = \frac{1}{49}(1 - V)^{-3} \left\{\frac{7}{3}(4V - 3)\right\}^{9/11} \left\{\frac{7}{17}(5 - 3V)\right\}^{116/33}. \quad (10)$$

The pressure ration  $p/p_2$  tends to a constant as  $\zeta \rightarrow 0$ , while  $\beta/\beta_2 \propto \zeta$ ,  $\rho/\rho_2 \propto \zeta^9$  in this limit.

### 3. Numerical Results

#### 3.1. Initial Conditions

We consider an initial uniform spherical fireball surrounded by a uniform cold ISM. The initial conditions are determined by four parameters: the total energy  $E$ , the baryonic mass  $M_0(= E/\eta)$  and the radius  $R_0$  of the fireball and the ISM density  $\rho_1$ . A “cold” ISM means that its pressure is negligible compared to the pressure behind the shocks throughout the whole evolutions. For convenience, we set the initial time as  $R_0$  rather than zero. We have chosen two sets of initial conditions to represent the the RRS and the NRS cases:  $E = 10^{52}\text{erg}$ ,  $\rho_1 = 1\text{proton cm}^{-3}$ ,  $\eta = 50$  and  $R_0 = 3 \times 10^{10}\text{cm}$  for the NRS case ( $\xi = 43$ ), and  $E = 10^{52}\text{erg}$ ,  $\rho_1 = 1\text{proton cm}^{-3}$ ,  $\eta = 10^4$  and  $R_0 = 4.3 \times 10^9\text{cm}$  for the RRS case ( $\xi = 0.1$ ).

We assume that the fluid is described by a constant adiabatic index  $\hat{\gamma} = 4/3$  although in reality this is not always true. The shell’s matter may cool during the coasting phase. However at the end of the coasting stage, the reverse shocks heat the fireball shell, and the ISM shocked by the relativistic forward shock carries most of the energy  $E$ . The main part of the system is subject to relativistic particles again. The forward shock is decelerated as  $\Gamma \propto R^{-3/2}$  and it becomes Newtonian at  $l$ . After that the scaling laws in the Newtonian regime depends on the adiabatic constant. But even then the shocked electrons will remain relativistic for a long time after this transition and the adiabatic index will remain around  $4/3$ .

### 3.2. Numerical Results

Figures 2,3 depict the evolutions of the Lorentz factors for the NRS and the RRS cases, respectively. One clearly sees the initial acceleration phase in which the Lorentz factor increases linearly with time. This is followed by a coasting phase in which the Lorentz factor is a constant:  $\eta$ . This stage ends when the effect of ISM becomes significant and most of the kinetic energy is dissipated at  $R_\gamma$  or  $R_\Delta$ . Then a self similar phase begins in which the Lorentz factor of the forward shock decreases like  $\Gamma \propto R^{-3/2}$ . At  $l$  the solution becomes non relativistic and it turns into the Sedov-Taylor solution. A difference appears between the NRS and the RRS fireballs only in the energy transfer phase. As expected a sharp decrease in  $\gamma$  is seen in the RRS case. A more gradual transition is seen in the NRS case.

In the following sections we compare the numerical results with the analytic estimates. We examine the validity of the estimates of  $R_L$ ,  $R_s$ ,  $R_\Delta$ ,  $R_\gamma$ ,  $R_N$  and  $l$  as indicators of transition scales.

#### 3.2.1. Free Acceleration Stage

A highly relativistic shell is formed after a short acceleration phase (see figure 4). The width of the shell is constant in this acceleration stage (figure 5). The density and the pressure peak at the same position in the local fluid frame. In the observer frame, the outer part of the shell has a higher Lorentz factor and the density peak is wider than the pressure peak. The density peak (dotted line) moves ahead of the pressure peak (solid line) in the observer frame (figure 5).

The average Lorentz factor of the each fluid element in the shell increase as the radius of the shell increases,  $\gamma \sim r/\Delta$ . However, the Lorentz factor of the outermost layers is

well above the average. This is results from the initial sharp edges of the fireball. The initial acceleration of the outermost layers depends on the steepness of the initial pressure distribution at the edge of the fireball. The initial step function distribution that we have chosen leads to large acceleration of the outermost layers. We can regard the thin region at the boundary of the fireball as expanding in the free expansion velocity, independent of the fireball thickness  $\Delta$ . However, this fast layer is thin and its mass is negligible. Except of the evolution of the maximal Lorentz factor (at the outermost layers) the evolution of the bulk of the fireball is not effected by the choice of the initial steepness of the boundary. The initial conditions are washed out later, when the interaction with the ISM is significant, and even the maximal Lorentz factor is then independent of the initial conditions. Therefore we do not discuss this maximal value, but instead we consider the average Lorentz factor over the “uniform shell”. We define the average value as:

$$\langle f \rangle \equiv \int f m r^2 dr / \int m r^2 dr, \quad (11)$$

where  $m \equiv \gamma \{\rho + (3 + \beta^2)p\}$  is the effective mass density in the observer frame and the integrals are defined from the origin to a radius at which the Lorentz factor takes the maximal value. The evolution of the average Lorentz factor  $\langle \gamma \rangle$  for the NRS and the RRS cases is shown in figure 2 and 3 (thick line) respectively. The Lorentz factors increase linearly with time. The average internal energy and the mass density in the observer frame are shown in figure 6.  $R_L$  is a good indicator to the transition from the acceleration stage to the coasting stage. The mass density equals the internal energy density at  $\sim R_L$  (see figure 6).

### 3.2.2. *Coasting Stage*

After the fireball uses up all the internal energy at  $R_L$ , it coasts with a Lorentz factor  $\eta$  (see figures 2 and 3). In the RRS case the shell has a frozen radial profile through this

stage, while in the NRS case the frozen pulse approximation breaks down at  $R_s$  and the shell begins to expand before the ISM has most of the system energy at  $R_\gamma$  (see figure 5). We can see the transition of the scaling laws of the density and the pressure at  $R_s$  in figure 6.

### 3.2.3. Energy Transfer Stage: The RRS Case

In the RRS case the reverse shock becomes relativistic at  $R_N$  before it crosses the shell at  $R_\Delta$ . From this moment onwards the Lorentz factor of the coasting shell is reduced considerably after the passage of the reverse shock. Figure 7 shows the deceleration by a relativistic reverse shock. There are four regions in the figure: the ISM, the shocked ISM, the shocked shell and the unshocked shell, which are separated by the forward shock (FS), the contact discontinuity (CD) and the reverse shock (RS).

Using the shocks' jump conditions and the equality of the pressure and the velocity at the contact discontinuity, we can estimate the Lorentz factor of the shocked region,  $\gamma_{CD}$ , and the Lorentz factor of the reverse shock,  $\Gamma_{RS}$ , for a planar geometry (Sari & Piran, 1995),

$$\gamma_{CD} = f^{1/4} \sqrt{\gamma_4/2}, \quad \Gamma_{RS} = \gamma_{CD}/\sqrt{2}, \quad (12)$$

where  $f \equiv \rho_4/\rho_1$ . The quantities just ahead of (or just behind) the reverse shock are denoted by the subscript 4 (or 3). For spherical geometry, the pressure is not constant in the shocked region bounded by the two shocks. The ratio  $f$  in the above equations should be replaced with  $(p_2/p_3)f$ . However, in our simulations,  $p_2/p_3$  is a factor of a few at most. Then, equation (12) can roughly explain the numerical result. The time it takes for the reverse shock to cross a distance  $dx$  in the shell material is  $dt = dx\gamma_4\sqrt{f}/2$ . As the reverse shock compresses the shell material, the width  $dx$  becomes  $dx/2$  after the shock passes through it. Then, the distance between the contact discontinuity and the reverse shock is

$t/2\gamma_4\sqrt{f}$  ( $\propto t^2$ ). Figure 8 shows the numerical result.

The relativistic reverse shock passes through the shell as  $t^2$  and it decelerates the coasting shell drastically. After this drastic deceleration, the shocked shell slows down as  $t^{-1/2}$  (figure 3) due to the pressure difference between  $p_2$  and  $p_3$ . At  $R_\Delta$  when the reverse shock crosses the shell,  $\gamma_{CD}$  reaches effectively the value of  $\gamma_2$  expected from the relativistic self similar solution and the profile of the shocked ISM region begins to approach the self similar one. The transition into the self similar solution is shown in figure 9.

At the beginning of the self similar deceleration stage, the density of the shocked shell is much larger than that of the shocked ISM. There is a large gap of the density at the contact discontinuity. However, the density perturbation, as we discuss in section 4, does not effect  $\gamma$  and  $p$ , and it does not propagate in the local fluid frame. Then, as the blast wave expands, it leaves the gap, and the ratio between  $\rho_2$  and the density of the shocked shell damps.

#### 3.2.4. Energy Transfer Stage: The NRS Case

In the NRS case ( $\xi > 1$ ), the shell begins to spread at  $R_s$  and the value of  $\xi$  decreases. At  $R_\gamma$ , a coincidence  $R_\Delta = R_\gamma = R_N$  happens. The shocked ISM becomes the main component of the system and the profile approaches the Blandford-McKee solution. At this stage the reverse shock is just mildly relativistic, the shell's Lorentz factor changes by a factor of order unity (see figure 10).

### 3.2.5. *Relativistic Self Similar Deceleration Stage*

In the deceleration stage, the hydrodynamic profiles of the shocked ISM depends on only  $E$  and  $\rho_1$ . The numerical values of the Lorentz factor  $\gamma_2$ , the density  $\rho_2$  and the pressure  $p_2$  just behind the shock are compared with the self similar solution in figure 11. The numerical result of Lorentz factor is consistent with the Blandford-McKee self similar solution within a few % difference in the relativistic regime (see figure 11 (b)). Though the density and the pressure peaks are narrower than the velocity peak (see equation (7)) and the numerical errors are larger, the density and the pressure agree with the analytic estimates within  $\sim 20\%$ . In the RRS case,  $\gamma_2$  begins to satisfy the relativistic self similar scaling at  $R = 1.9R_\Delta$  (circle 1 in figure 11 (b)). The self similar solution and the equation (6) with a factor  $1/2\pi^{1/4}$  which we neglected for simplicity, give the analytic estimate  $1.5R_\Delta$ . In the NRS case,  $\gamma_2$  reaches within a 10% error line at  $R = 2.4R_\gamma$ .

Flow profiles are plotted as a function of the similarity variable  $\chi$  in figure 12. In the top panel of the figure, the value of the Lorentz factor just behind the forward shock is  $\sim 15$ , and the value drops to  $\sim 5$  in the inner region. The numerical results agree well with the self similar solution. In the bottom panel of the figure, the value of the Lorentz factor just behind the forward shock is  $\sim 8$ , and the value drops to  $\sim 2$  at the inner region where the numerical results deviate from from the self similar solution. The relativistic self similar solution is derived with an assumption that each fluid element is highly relativistic, but it is a good approximation still at  $\gamma \sim 5$ .

### 3.2.6. *Transition to the Sedov-Taylor Solution*

The Lorentz factor of the forward shock decreases and it becomes non-relativistic around  $l(\sim 1.9 \times 10^{18}$  in this case). The scaling laws of the velocity  $\beta_2$ , the density  $\rho_2$  and

the pressure  $p_2$  also gradually shift from the Blandford-McKee solution to the Sedov-Taylor solution around  $l$  (see figure 11). The circles 2 ( $R_{c2} \equiv 0.46l$ ) and 3 ( $R_{c3} \equiv 0.61l$ ) in figure 11 (b) give a rough estimate of the radii where the relativistic self similar solution becomes invalid and the Newtonian self similar solution becomes valid ( $\gamma_2 \sim 1.9$  at circle 2,  $\beta_2 \sim 0.70$  at circle 3). The relation between  $\beta_2$  and  $R$  in the Newtonian self similar solution is already valid at circle 3, but the shock radius  $R$  is still proportional to time  $t$  at this stage and it is smaller than the radius expected by the Newtonian self similar solution. The relation between  $\beta_2$  and  $t$  in the Newtonian self similar solution becomes valid at circle 4 ( $R_{c4} \equiv 1.8l$ ) where  $\beta_2 = 0.14$ .

The transition of the profiles in the shocked ISM region, from the relativistic stage to the Newtonian stage, is shown in figure 13. The jump condition for a strong shock gives a simple relation between the ISM density  $\rho_1$  and the shocked density  $\rho'_2 (= \rho_2 \gamma_2)$  measured in the observer frame,  $\rho'_2 = \gamma_2(4\gamma_2 + 3)\rho_1$ . If ISM have been swept up at a radius  $R$ , the thickness of the blast wave is approximately  $R/\gamma_2(4\gamma_2 + 3) \propto R^4$  for the relativistic stage. The thickness is  $\propto R$  for the Newtonian stage. As the blast wave expands, it becomes broader (figure 13a). The inner part of the distribution begins to approach the Newtonian self similar one Around  $R_{c3}$  (figure 13b). The density profile approaches the one expected by the Newtonian self similar solution at  $R_{c3}$  (see figure 13c). The pressure profile approaches the Newtonian one more gradually and it still evolves after  $R_{c3}$  (figure 13d). The velocity and pressure profiles are consistent with the analytic estimates within 10% level at  $R_{c4}$ .

#### 4. Evolution of Perturbations to Blandford-McKee Solution

The simulations presented in the previous sections have shown that the hydrodynamical profiles of the shocked ISM approaches the relativistic self similar Blandford-McKee solution at the end of the energy transfer phase. It implies that the self similar solution is attractive

and stable. In this section we consider the evolution of spherical perturbations to the self similar profile.

For an infinite uniform fluid there are two types of perturbations in the linear theory. One type is a sound wave propagating with the sound velocity relative to the fluid. The other is an entropy-vortex wave moving with the fluid. It is an entropy perturbation with no change of the pressure and it includes a spherical density perturbation.

As an unperturbed initial configuration we take a self similar blast wave with a total energy  $E = 10^{52}$  erg in a uniform ISM of the density 1 proton / $cm^3$ , at the moment where the Lorentz factor behind the shock is  $\gamma = 4000$  ( $t \sim 5.3 \times 10^{15}$ ). We then add a Gaussian perturbation  $\delta q/q = \delta \exp[-(\chi - \chi_0)^2/\Delta\chi^2]$ , with  $\delta = 1$ ,  $\chi_0 = 3$  and  $\Delta\chi = 0.5$  to one of the hydrodynamical variables: the Lorentz factor, the density or the pressure.  $q$  stands for these variables and  $\delta q$  for its perturbation. Figures 14 (a), (b) and (c) depict the flow profiles as functions of  $\chi$  for the perturbation of  $\rho$ ,  $\gamma$  and  $p$ , respectively. The dashed lines are the initial profile (self similar solution + perturbation), and the solid lines are at  $\delta t = 4.3 \times 10^{14}$ sec later.

The density perturbation (figure 14 (a)) does not effect other quantities ( $\gamma$  and  $p$ ) and it does not propagate in the local fluid frame. We use the self similar solution to estimate the evolution of  $\chi_e$  of the fluid element in the perturbed region (or any other fluid element). Taking the derivative of  $\chi_e$  along its line of flow we get  $d\chi_e/dt = 4(\chi_e + 1)/t$  so that a fluid element which had been at  $\chi_0$  at a time  $t_0$ , will be at  $\chi_e(t) \sim \chi_0(t/t_0)^4$ . The fluid element which had a density  $\rho_0$  at  $t_0$ , will have a density  $\rho_e(t) = \rho_0(t/t_0)^{-13/2}$ . The ratio between the density perturbation  $\delta\rho_e(t, r(t))$  and the unperturbed value  $\rho_e(t, r(t))$  is constant in time, but the perturbation will depart from the forward shock as  $\chi_e \propto t^4$  and the perturbation becomes less important as  $\rho_e/\rho_2 \propto t^{-5}$ . Our numerical results agree well with these scalings.

A velocity perturbation (figure 14 (b)) induces pressure and density perturbations.

The pulse of the coupled perturbations is decomposed after a short time into two pulses: An outgoing compression pulse (outgoing motion corresponds to a decreasing  $\chi$ ) and an ingoing rarefaction pulse (a rarefaction wave and a shock wave). These waves propagate with the speed of sound in the local fluid frame  $\gamma'_s = \sqrt{4p_e/3\rho_e} = 2\gamma_2^{1/2}\chi^{-1/12}/3$ . The speed of the outgoing and the ingoing sound wave in the observer frame are  $\gamma_s = 4\gamma_2^{3/2}\chi^{-7/12}/3$  and  $3\gamma_2^{1/2}\chi^{-5/12}/4$ , respectively. Assuming that the initial position  $\chi_0$  of the perturbation at a time  $t_0$  is not too far from the forward shock,  $\gamma_s \gg \Gamma$ , we get the position of the outgoing pulse  $\chi = \chi_0(t/t_0)^{-4}$ . The pulse reaches the forward shock at  $t = \chi_0^{1/4}t_0$  and it boosts the forward shock. The position of the ingoing pulse cannot be expressed by a simple analytic formula, but it departs from the forward shock much faster than a density perturbation. After the out-going pulse boosts the forward shock, the flow profile is almost the self similar one.

A pressure perturbation (figure 14 (c)) also induces perturbations in  $\gamma$  and  $\rho$ . The perturbations consist of three components, two propagating component and a standing density perturbation. After an outgoing compression pulse and an ingoing shock propagate, a density perturbation still stays at the position where the initial pressure perturbation was (in the local fluid frame). The ingoing shock leaves the forward shock quickly. The density perturbation departs from the forward shock as discussed earlier. The outgoing pulse is basically the same one appearing in the case of an initial velocity perturbation. The pulse boosts the forward shock and at this stage the profile is almost the self similar one.

## 5. Conclusions

We have explored numerically the evolution of a relativistic fireball interacting with a uniform ISM, through the stages of initial acceleration, coasting, energy transfer to the ISM and the deceleration. These calculations begin when the fireball is at rest. They follow the

acceleration to a relativistic velocity and the subsequent slowing down to a velocity far below the speed of light. These calculations span more than eight orders of magnitudes in the size of the fireball. The current analytic understanding of the fireball evolution can explain well our numerical results. Initially, the Lorentz factor increases linearly with the radius during the initial free acceleration stage. At  $R_L$  the fireball has transferred all its initial radiation energy to kinetic energy and it coasts. Then the energy is transferred to the ISM. This takes place at  $R_\gamma$  for the NRS case, or at  $R_\Delta$  for the RRS case. After that the shocked ISM carries most of the initial energy of the fireball. The profile of the shocked ISM is then described well by the relativistic self similar Blandford-McKee solution. The forward shock decelerates as  $\Gamma \propto R^{-3/2}$  and it becomes Newtonian at  $l$ . After that the non-relativistic self similar Sedov-Taylor solution sets in. We have shown that the relativistic self similar solution is an excellent approximation, down to  $\gamma \sim 5$  and a reasonable approximation even down to  $\gamma \sim 2$ . We have also examined the transition into the relativistic self similar solution, and the transition from this solution to the non-relativistic self similar solution.

With the spherical code, we have shown that the hydrodynamical profiles of the shocked ISM approaches to the relativistic self similar solution at the end of the coasting stage, even though the initial conditions of the simulation do not have self similar profiles. It implies that the relativistic self similar solution is attractive and stable for a spherical perturbation. We have tracked the evolution of the spherical density, velocity and pressure perturbations to the relativistic self similar solution in order to verify the stability of this solution.

The Blandford-McKee solution is the basis of much of the GRB afterglow theory. It is used to obtain an explicit expression for the radial profile during the deceleration stage. We have shown that this model is reasonable even down to  $\gamma \sim 2$ . It is also valid even in the case of a radial inhomogeneity in the ISM.

Though the results presented in this paper are intended as a more general explanation of the strong explosion problem rather than a detailed fits of the GRB afterglow, comparisons of the numerically predicted light curves based on this computations in detailed realistic models with the recent and upcoming observations will enable us to determine free parameters in the GRBs model that cannot be calculated from first principles, such as the total energy of the system, the surrounding density, the fraction of the energy that is given by the shocks to electrons or to the magnetic field.

S.K. gratefully acknowledges the support by the Golda Meir Postdoc fellowship. R.S. thanks The Clore Foundations for support. This work was supported in part by a US-Israel BSF grant 95-328 and by a NASA grant NAG5-3516.

## References

- Blandford,R.D. & McKee,C.F. 1976, Phys. of Fluids, 19, 1130.
- Daigne, F. & Mochkovitch, R. 1997, preprint.
- Goodman,J. 1986, ApJ, 308, L47.
- Kobayashi,S., Piran,T. & Sari,R. 1997, ApJ, 490, 92.
- Landau,L.D. & Lifshitz,E.M. 1987, Fluid Mechanics 2nd ed. (Pergamon Press), Chap. X.
- Katz, J., 1994, ApJ, 422, 248..
- Mészáros,P., Laguna,P. & Rees,M.J. 1993, ApJ, 415, 181.
- Mészáros,P. & Rees,M.J. 1992, ApJ, 397, 570.
- Narayan,R., Paczyński,B. & Piran,T. 1992, ApJ, 395, L83.
- Paczyński,B. 1986, ApJ, 308, L51.
- Piran,T., Shemi,A. & Narayan,R. 1993, MNRAS, 263, 861.
- Rees,M.J. & Mészáros, P. 1994, ApJ, 430, L93.
- Sari,R. 1997, ApJ, 489, L37.
- Sari,R. & Piran,T. 1995, ApJ, 455, L143.
- Sari,R. & Piran,T. 1997, ApJ, 485, 270.
- Sedov,L.I. 1946, Prikl. Mat. i Mekh.,10, 241
- Shemi,A. & Piran,T. 1990, ApJ, 365, L55.
- Taylor G.I. 1950, Proc. Roy. Soc. London, A201, 159.
- Von Neumann J. 1947, Los Alamos Sci. Lab. Tech. Series, Vol 7.

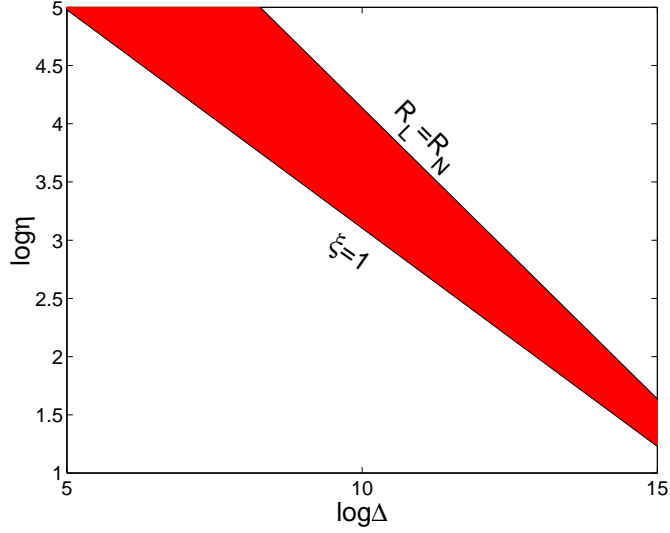


Fig. 1.— Allowed parameter region for  $l = 1.9 \times 10^{18}\text{cm}$  ( $E = 10^{52}\text{ergs}$  and  $\rho_1 = 1\text{proton}/\text{cm}^3$ ). The line ( $\xi = 1$ ) separates the NRS case (lower left) and the RRS case (upper right).  $R_L < R_N$  is the lower left region of the line ( $R_L = R_N$ ).

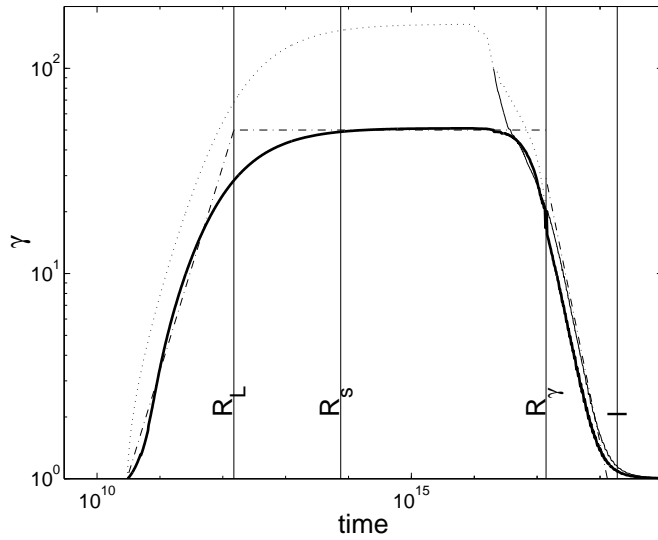


Fig. 2.—  $\gamma$  vs Time, for the NRS case ( $\xi = 43$ ,  $E = 10^{52}$  erg,  $\eta = 50$   $R_0 = 3 \times 10^{10}\text{cm}$ ). The average value (thick solid line), the value just behind the forward shock (thin solid line), the maximal value (dotted line) and the analytic estimate (dashed dotted line).

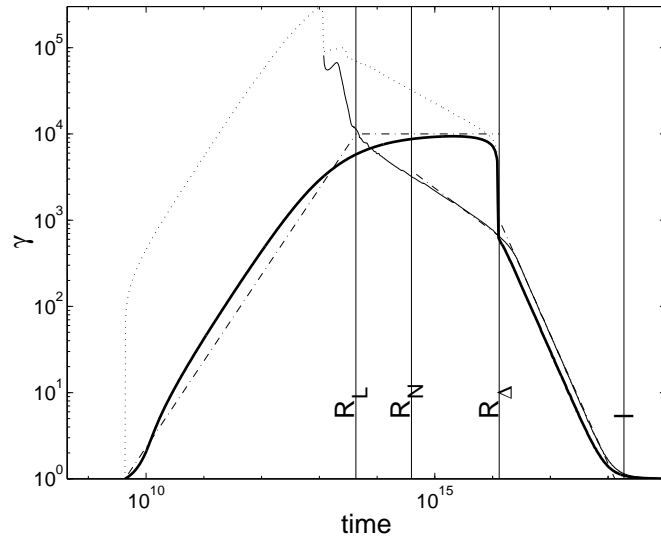


Fig. 3.—  $\gamma$  vs time for the RRS case ( $\xi = 0.1$ ,  $E = 10^{52}$  erg,  $\eta = 10^4$   $R_0 = 4.3 \times 10^9$  cm). The average value (thick solid line), the value just behind the forward shock (thin solid line), the maximal value (dotted line) and the analytic estimate (dashed dotted line).

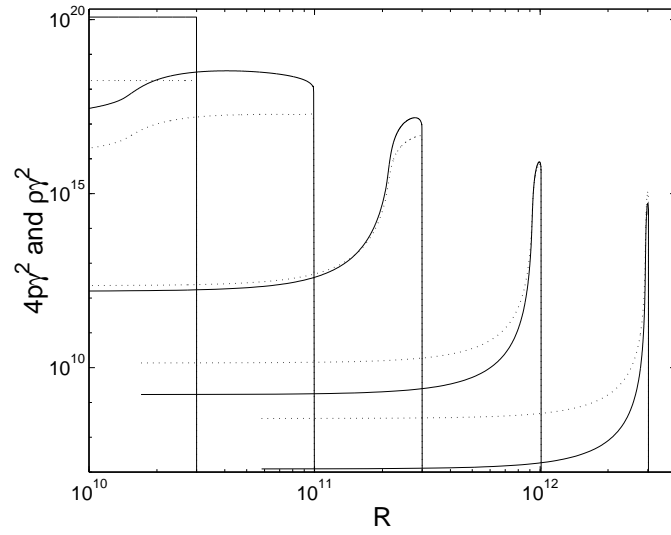


Fig. 4.— Profiles of the internal energy density  $4p\gamma^2$  (solid line) and the mass density  $\rho\gamma^2$  (dotted line) in the frame of ISM during the initial acceleration stage (internal energy dominated stage to matter dominated stage). The initial parameters are similar to those in figure 2)

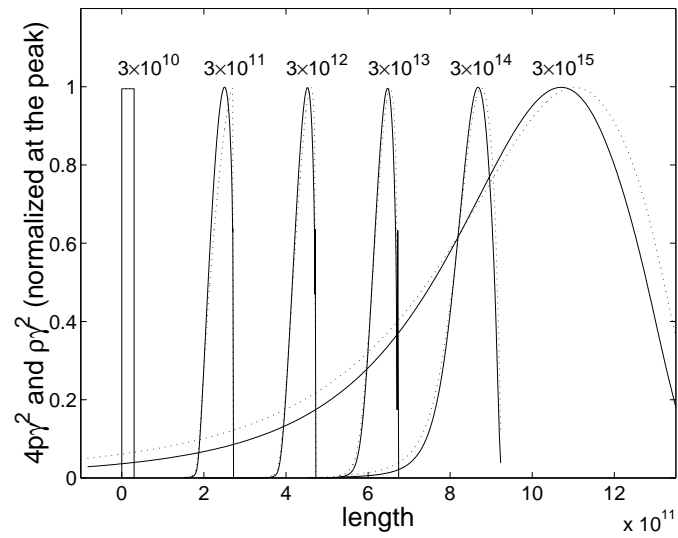


Fig. 5.— The shell structures at different times in the acceleration and coasting stage. The internal energy density  $4\gamma^2$  (solid line) and the mass density  $\rho\gamma^2$  (dotted line) normalized at the peaks. The initial parameters are similar to those in figure 2) The initial time is set as  $R_0(= 3 \times 10^{10})$ .

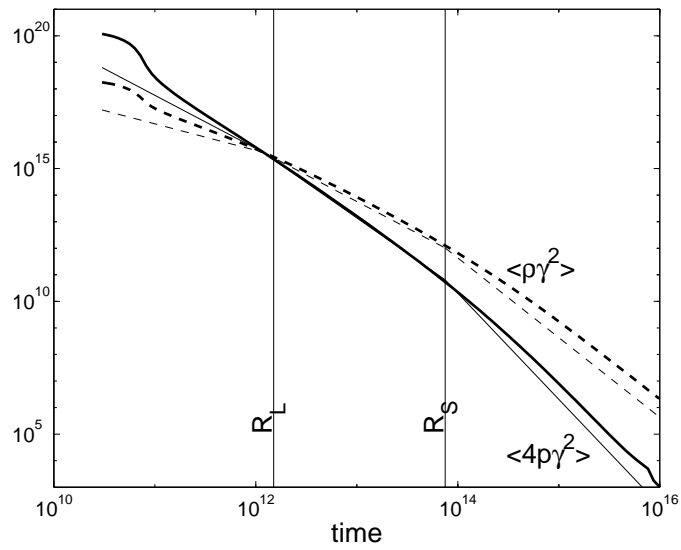


Fig. 6.— The average internal energy density  $4p\gamma^2$  (thick solid line), the average mass density  $\rho\gamma^2$  (thick dashed line) and an analytical estimate of the internal energy density (thin solid line) and the mass density (thin dashed line). The latter are normalized at the cross point of the numerical results. The initial parameters are the same as in figure 2.

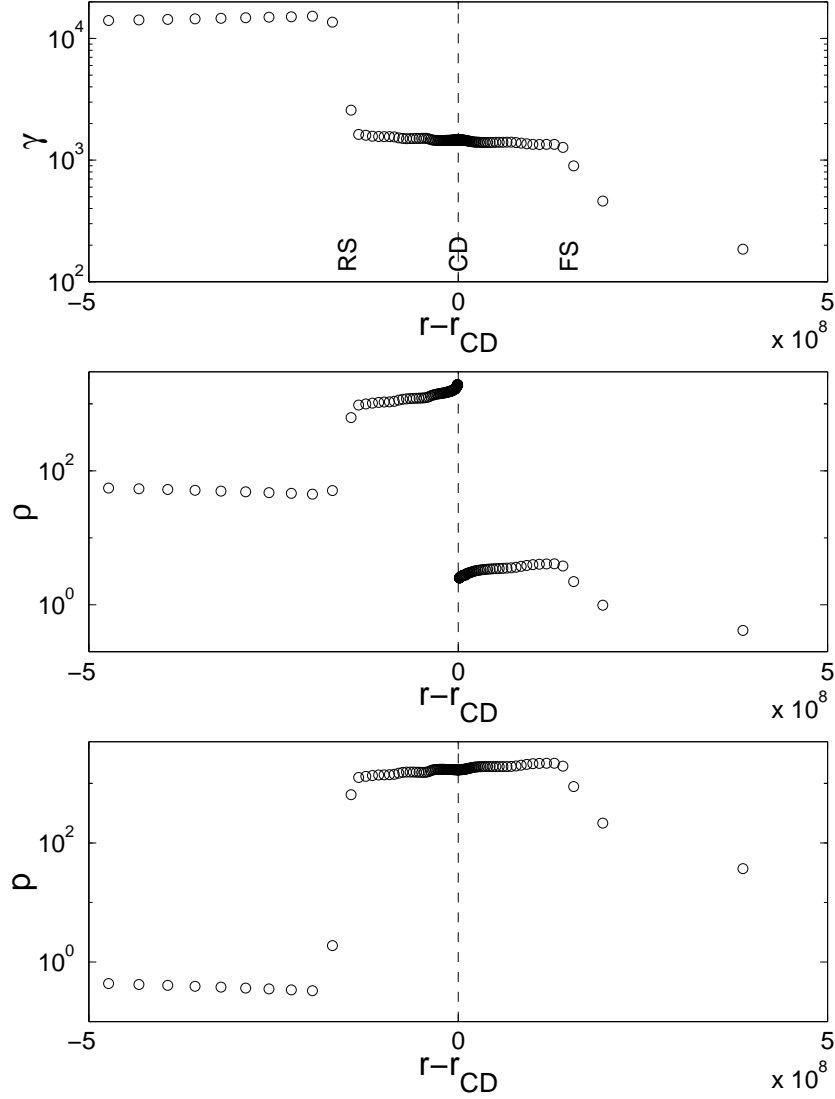


Fig. 7.— : The Lorentz factor  $\gamma$ , density  $\rho$  and pressure  $p$  in the deceleration stage by the reverse shock ( $t = 3 \times 10^{15}$ ) for an RRS solution. The x axis is the distance from the contact discontinuity (dashed line). RS and FS indicate the positions of the reverse shock and the forward shock, respectively. The initial parameters are the same as in figure 3.

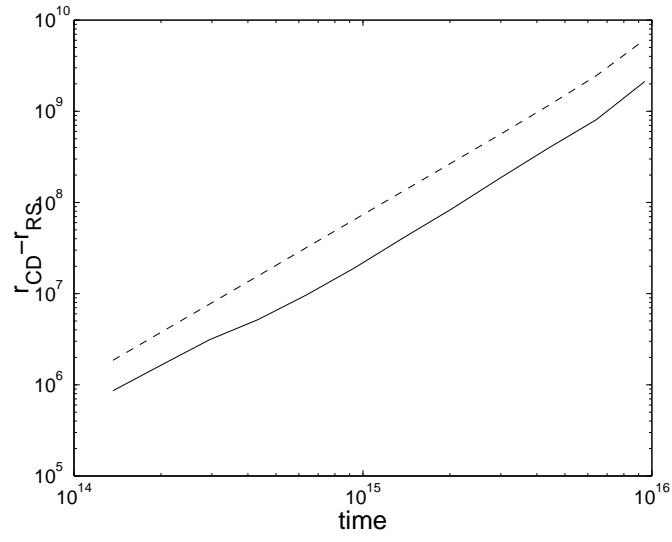


Fig. 8.— The distance between the contact discontinuity and the reverse shock as a function of time:  $r_{CD} - r_{RS}$  (solid line),  $t/2\gamma_4\sqrt{f}$  (dashed line) for a RRS solution. The initial parameters are the same as in figure 3.

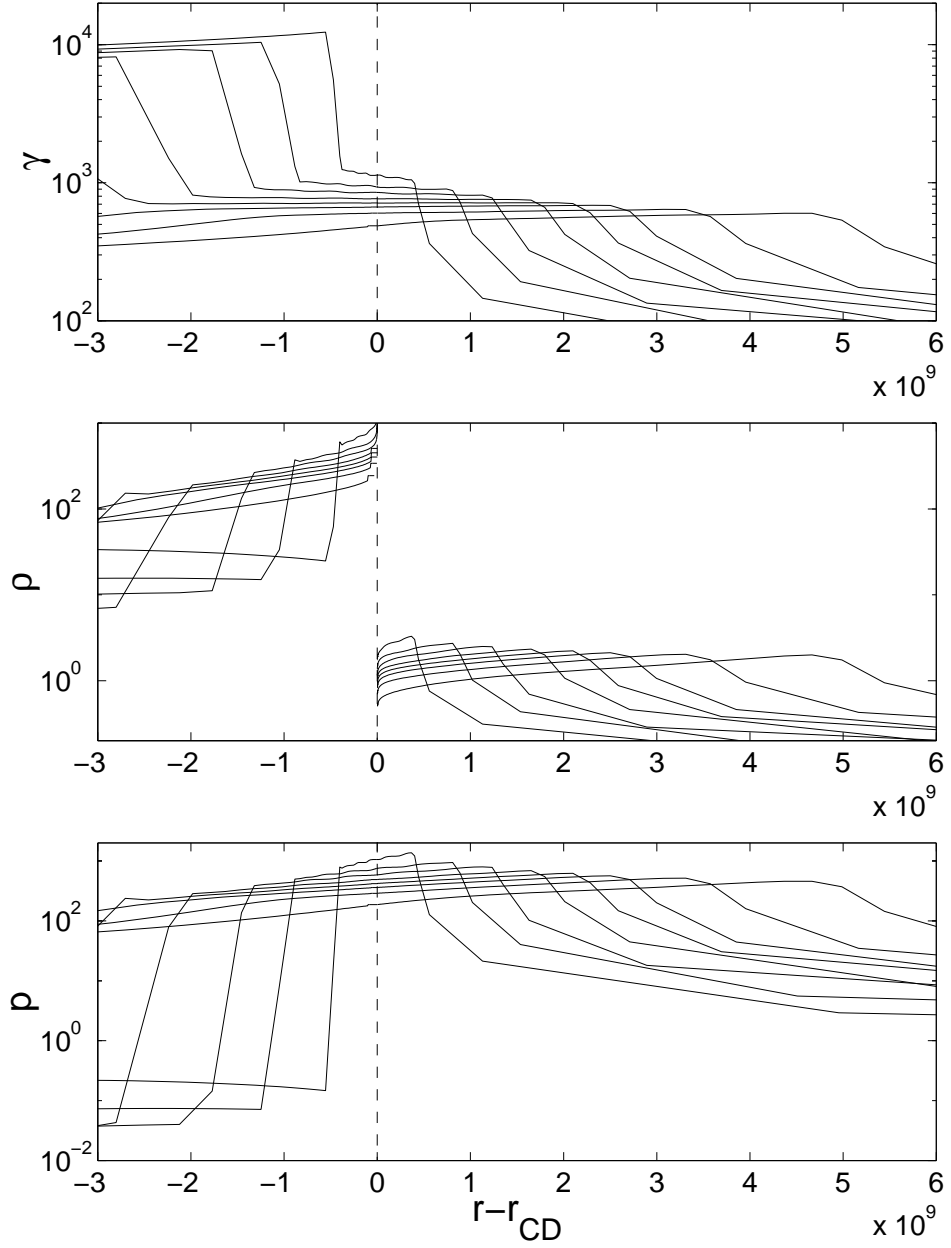


Fig. 9.— The transition into the Relativistic self similar solution in a RRS solution. Profiles of  $\gamma$ ,  $\rho$  and  $p$  at different times ( $t = 0.41R_\Delta$ ,  $0.60R_\Delta$ ,  $0.73R_\Delta$ ,  $0.85R_\Delta$ ,  $0.93R_\Delta$ ,  $R_\Delta$ ,  $1.1R_\Delta$  and  $1.2R_\Delta$ ) The x axis is the distance from the contact discontinuity (dashed line).

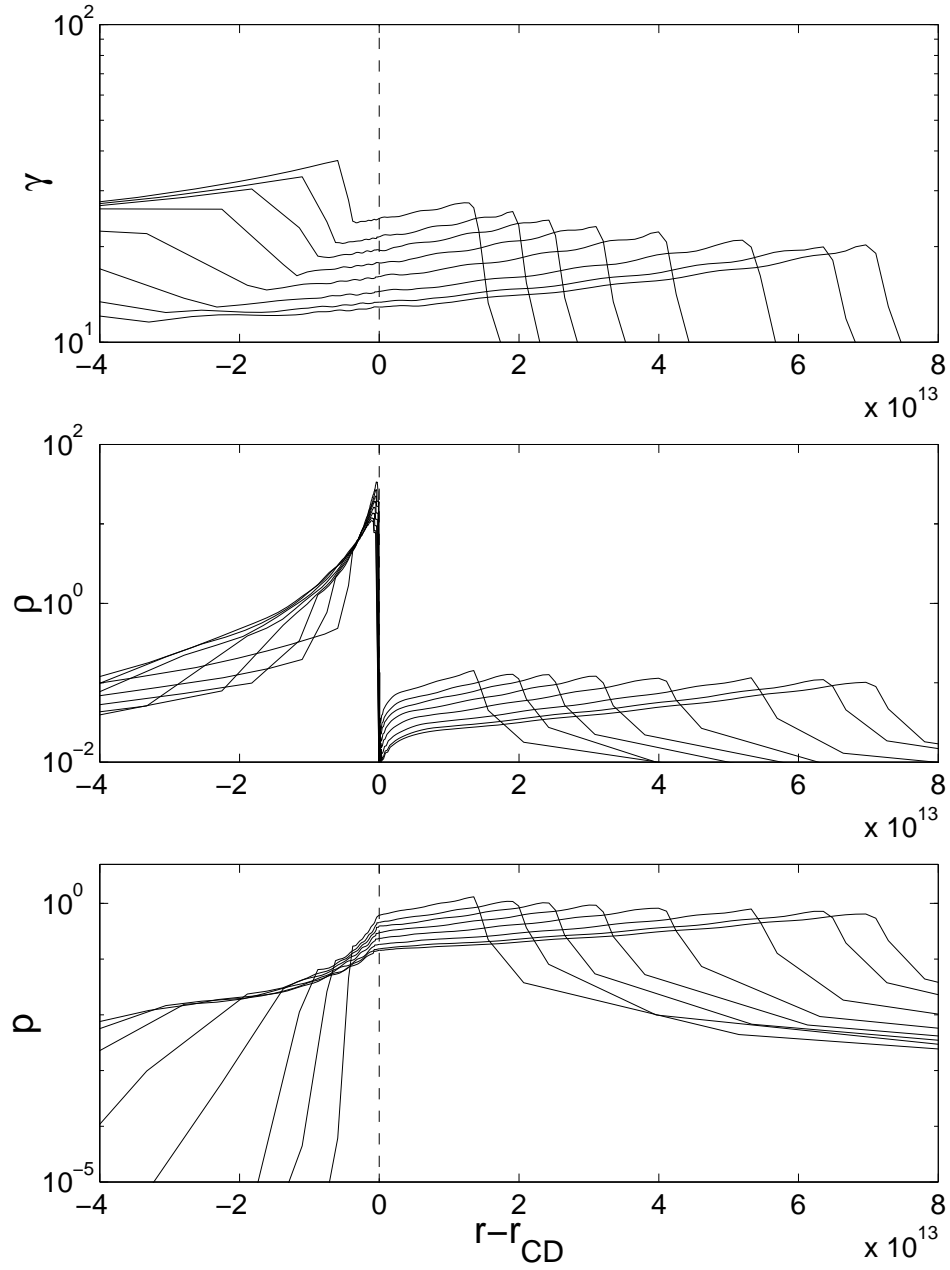


Fig. 10.— The transition into the Relativistic self similar solution for a NRS solution. Profiles of  $\gamma$ ,  $\rho$  and  $p$  at different times ( $t = 0.70R_\gamma, 0.77R_\gamma, 0.82R_\gamma, 0.87R_\gamma, 0.92R_\gamma, 0.98R_\gamma, R_\gamma,$  and  $1.1R_\gamma$ ) The x axis is the distance from the contact discontinuity (dashed line).

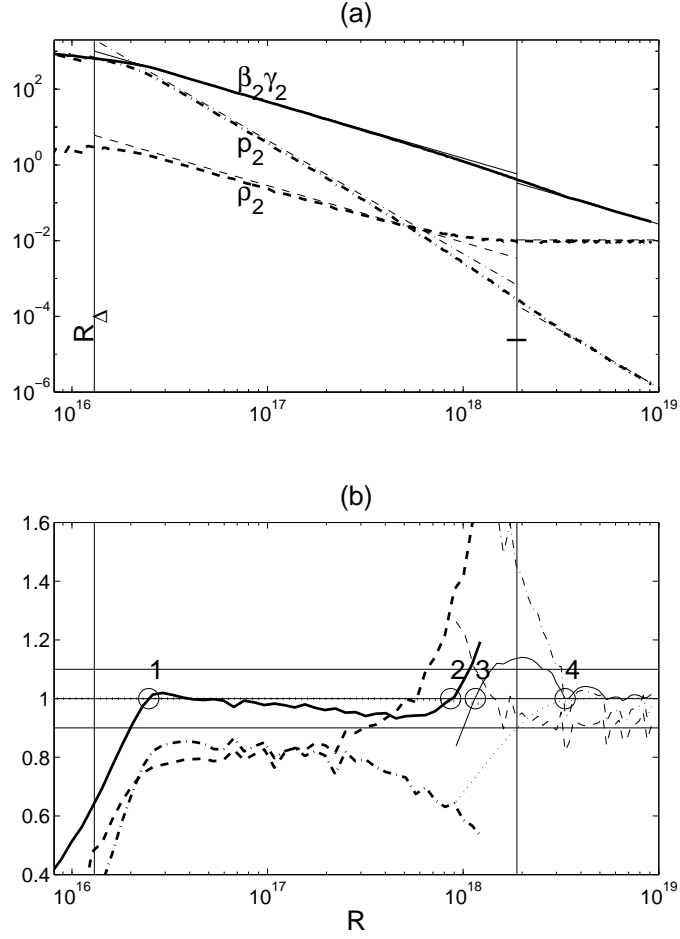


Fig. 11.— The deceleration stage. (a)  $\beta_2 \gamma_2$  (solid lines), density (dashed lines) and pressure (dashed dotted lines) just behind the shock vs the shock radius. The numerical results are thick lines and the relativistic and the Newtonian self similar solution are thin lines. We plot  $\gamma_2$  ( $\beta_2$ ) rather than  $\beta_2 \gamma_2$  for the relativistic self similar solution (the Newtonian self similar solution). The initial parameters are the same as in figure 3.

(b) The ratio between the numerical results and the analytic estimates.  $\gamma_2$  or  $\beta_2$  (solid line), density (dashed line) and pressure (dashed dotted line) just behind shock and the shock radius (dotted line). The numerical results are compared with the relativistic (thick line) or the Newtonian (thin line) self similar solution.  $\gamma_2$  ( $\beta_2$ ) is compared with the analytic estimate in the relativistic regime (the Newtonian regime). The circles 1,2,3 and 4 indicating the cross points are at  $R = 1.9R_\Delta, 0.46l, 0.61l$  and  $1.8l$  respectively.

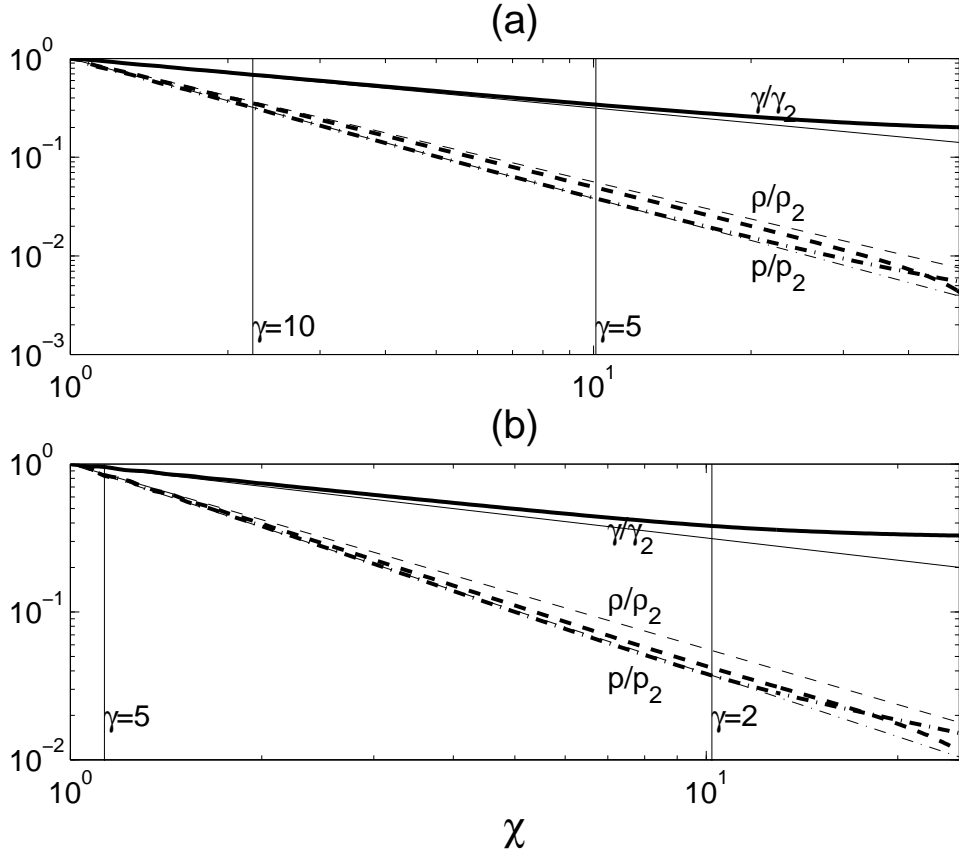


Fig. 12.— The Lorentz factor (solid lines), the density (dashed lines) and the pressure (dashed dotted lines) as a function of  $\chi$  during the relativistic deceleration stage at different times: (a)  $t = 2 \times 10^{17}$  ( $\gamma_2 \sim 15$ ) (b)  $t = 4 \times 10^{17}$  ( $\gamma_2 \sim 8$ ): The numerical results are thick lines and the analytical results are thin lines.  $\gamma$ ,  $\rho$  and  $p$  are normalized with the numerical results  $\gamma_2, \rho_2$  and  $p_2$ . The vertical lines indicate the positions where the fluid elements have the values of the Lorentz factor  $\gamma = 2, 5$  or  $10$ . The initial parameters are the same as in figure 3.

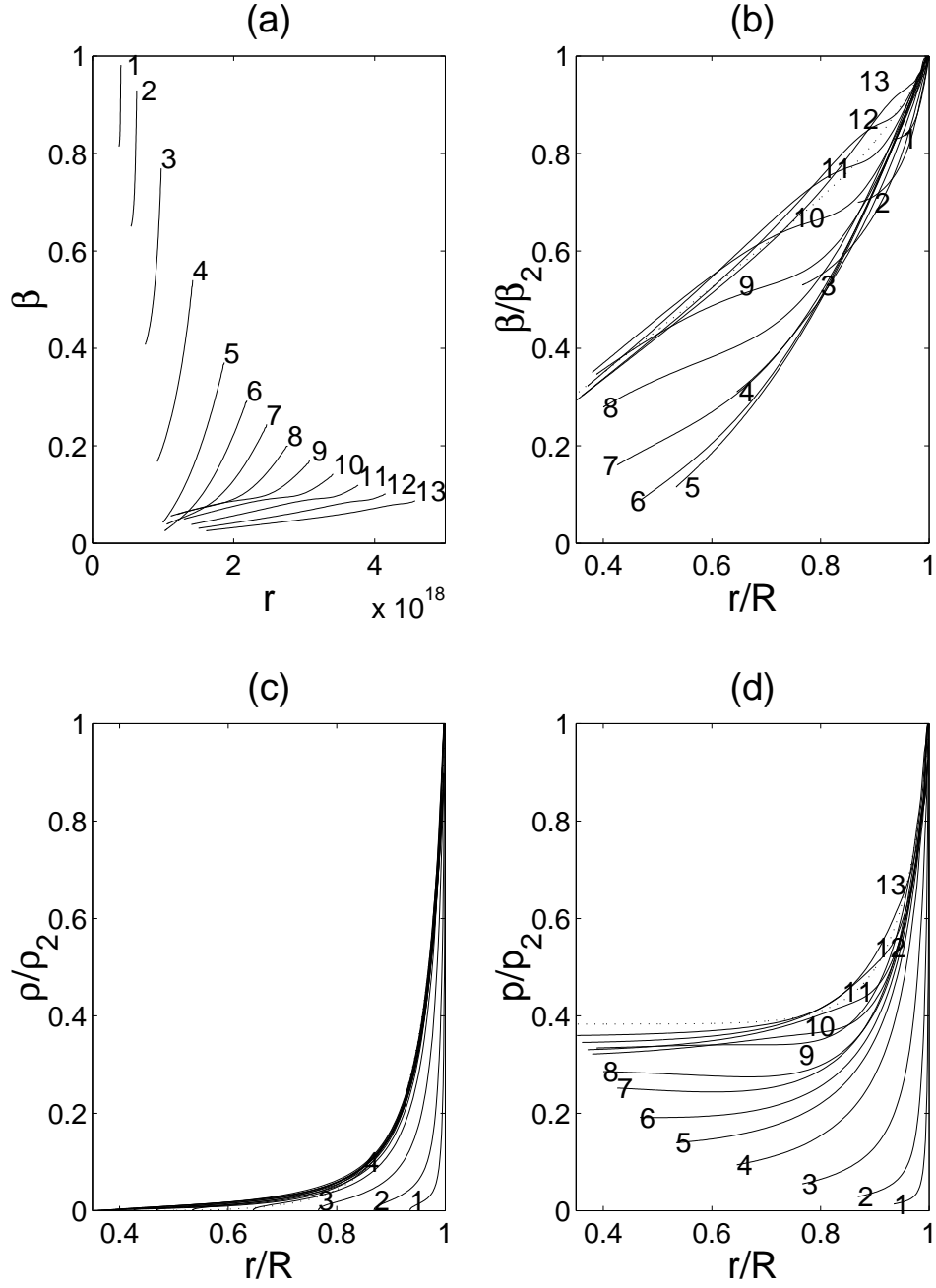


Fig. 13.— The transition of the flow profile of the shocked ISM from the relativistic Blandford-McKee solution to the Newtonian Sedov-Taylor solution: (a)  $\beta$  vs  $r$  (b)  $b/b_2$  vs  $r/R$  (c)  $\rho/\rho_2$  vs  $r/R$  and (d)  $p/p_2$  vs  $r/R$ . The dotted lines shows the Newtonian self similar solution. The number denote the shock radius  $R =$ : 1)  $0.21l$ , 2)  $0.33l$ , 3)  $0.52l$ , 4)  $0.76l$ , 5)  $1.0l$ , 6)  $1.2l$ , 7)  $1.3l$ , 8)  $1.5l$ , 9)  $1.6l$ , 10)  $1.8l$ , 11)  $2.0l$ , 12)  $2.2l$ , 13)  $2.4l$ . The initial parameters are the same as in figure 3.

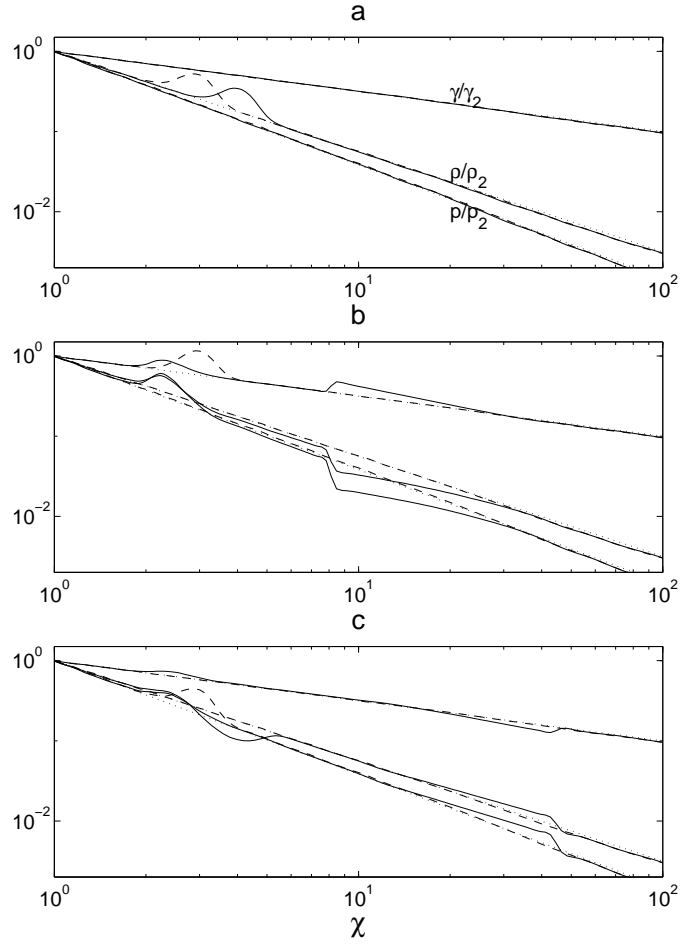


Fig. 14.— Stability of the Relativistic self similar solution. Perturbation of  $\rho$  - (a),  $\gamma$  - (b) and  $p$  - (c). Shown are the unperturbed self similar solution (dotted lines), the initial perturbed profiles (dashed lines) and the future evolution (solid lines)